

Activation of Calcium-dependent Chloride Channels in Rat Parotid Acinar Cells

JORGE ARREOLA,*¹ JAMES E. MELVIN,* and TED BEGENISICH[†]

From the *Departments of Dental Research and [†]Pharmacology and Physiology, University of Rochester Medical Center, Rochester, New York 14642

ABSTRACT The Ca^{2+} and voltage dependence of Ca^{2+} -activated Cl^- currents in rat parotid acinar cells was examined with the whole-cell patch clamp technique. Acinar cells were dialyzed with buffered free Ca^{2+} concentrations ($[\text{Ca}^{2+}]_i$) from <1 nM to $5 \mu\text{M}$. Increasing $[\text{Ca}^{2+}]_i$ induced an increase in Cl^- current at all membrane potentials. In cells dialyzed with $[\text{Ca}^{2+}]_i > 25$ nM, depolarizing test pulses activated a Cl^- current that was composed of an instantaneous and a slow monoexponential component. The steady-state current-voltage relationship showed outward rectification at low $[\text{Ca}^{2+}]_i$ but became more linear as the $[\text{Ca}^{2+}]_i$ increased because of a shift in Cl^- channel activation toward more negative voltages. The Ca^{2+} dependence of steady-state channel activation at various membrane voltages was fit by the Hill equation. The apparent K_d and Hill coefficient obtained from this analysis were both functions of membrane potential. The K_d decreased from 417 to 63 nM between -106 and $+94$ mV, whereas the Hill coefficient was always >1 and increased to values as large as 2.5 at large positive potentials. We found that a relatively simple mechanistic model can account for the channel steady-state and kinetic behavior. In this model, channel activation involves two identical, independent, sequential Ca^{2+} binding steps before a final Ca^{2+} -independent transition to the conducting conformation. Channel activation proceeds sequentially through three closed states before reaching the open state. The Ca^{2+} binding steps of this model have a voltage dependence similar to that of the K_d from the Hill analysis. The simplest interpretation of our findings is that these channels are directly activated by Ca^{2+} ions that bind to sites $\sim 13\%$ into the membrane electric field from the cytoplasmic surface. Key words: chloride secretion • chloride conductance • voltage dependence • kinetic model

INTRODUCTION

Fluid and electrolyte secretion is coupled to vectorial Cl^- movement (for reviews see Nauntofte, 1992; Petersen, 1992; Turner, 1993; Cook et al., 1994). In exocrine acinar cells, receptor-mediated secretory events are initiated by Cl^- loss induced by an increase in the concentration of intracellular Ca^{2+} ($[\text{Ca}^{2+}]_i$)¹ (Martinez and Cassity, 1986; Melvin et al., 1987; Merritt and Rink, 1987). The exit of Cl^- into the lumen via an apical pathway results in the production of a fluid rich in Cl^- . This apical Cl^- efflux pathway has not been unequivocally identified in salivary acinar cells, but by analogy to other epithelia, Cl^- channels are likely to be involved (for reviews see Frizzell and Halm, 1990; Anderson et al., 1992). The participation of Cl^- channels in the fluid and electrolyte secretion process of sal-

ivary glands has been inferred from the inhibition of Cl^- efflux by Cl^- channel blockers (Martinez et al., 1987; Melvin et al., 1987). In addition, Cl^- channel activation has been demonstrated in acinar cells exposed to Ca^{2+} -mobilizing agonists (Iwatsuki and Petersen, 1977; Petersen and Philpott, 1980; Iwatsuki et al., 1985; Evans and Marty, 1986; Gray, 1989; Ishikawa and Cook, 1993; Arreola et al., 1995a; Arreola et al., 1996). The expression of this type of channel is consistent with the Ca^{2+} dependence of fluid secretion (Douglas and Poisner, 1963; Martinez and Cassity, 1986; Cook et al., 1988). Consequently, Ca^{2+} -activated Cl^- channels are apparently a key element of the secretion process. However, the biophysical properties of these channels have not been studied sufficiently to establish adequately their role in secretion or to address the question of mechanisms of activation. At a minimum, details of the Ca^{2+} sensitivity and kinetic properties are required.

In this paper, we describe the Ca^{2+} and voltage dependence and the kinetics of Ca^{2+} -activated Cl^- channels in rat parotid acinar cells. Our results demonstrate that the Ca^{2+} sensitivity is in the nanomolar range and that Ca^{2+} may directly gate these Cl^- channels. The results indicate that two (or more) Ca^{2+} ions are required to activate a single Cl^- channel. We show that a simple model for the Ca^{2+} -dependent gating can account for the observed properties. The characteristics of this

Address correspondence and reprint requests to Dr. Ted Begenisich, Department of Pharmacology and Physiology, University of Rochester Medical Center, 601 Elmwood Avenue, Box 711, Rochester, NY 14642. Fax: (716) 461-3259; E-mail: tbb@crocus.medicine.rochester.edu

¹Abbreviations used in this paper: $[\text{Ca}^{2+}]_i$, free intracellular Ca^{2+} concentration; HEDTA, *N*-(2-hydroxyethyl)ethylenedinitrilo-*N,N,N'*-tri-acetic acid; NMDG, *N*-methyl-D-glucamine; TEA, tetraethylammonium; TES, *N*-tris(hydroxymethyl)methyl-2-aminoethanesulphonic acid.

channel make it a likely candidate for the apical Cl^- efflux pathway activated by increased intracellular Ca^{2+} during fluid secretion.

MATERIALS AND METHODS

Single-Cell Dissociation

Single acinar cells were dissociated from rat parotid glands as previously described (Arreola et al., 1995b). Briefly, glands were dissected from exsanguinated Wistar strain male rats (Charles River Laboratories, Kingston, NY) after CO_2 anesthesia. Glands were minced in Ca^{2+} -free, MEM (GIBCO BRL, Gaithersburg, MD) plus 1% BSA (Fraction V; Sigma Chemical Co., St. Louis, MO). The tissue was treated for 20 min (37°C) with a 0.02% trypsin solution (Ca^{2+} -free MEM, 1 mM EDTA, 2 mM glutamine, and 1% BSA). Digestion was stopped with 2 mg/ml of soybean trypsin inhibitor (Sigma Chemical Co.), and the tissue was further dispersed by two sequential treatments of 60 min each with collagenase (100 U/ml of type CLSPA; Worthington Biochemical Corp., Freehold, NJ) in Ca^{2+} -free MEM, 2 mM glutamine, and 1% BSA. The dispersed cells were centrifuged and washed with basal medium Eagle (GIBCO BRL)/BSA-free. The final pellet was resuspended in basal medium Eagle/BSA-free plus 2 mM glutamine and plated onto poly-L-lysine-coated glass coverslips.

Whole-Cell Recording

The whole-cell configuration of the patch clamp technique (Hamill et al., 1981) was used to record currents from single parotid acinar cells plated on poly-L-lysine-coated coverslips. Glass pipettes were fabricated to have 1–2 M Ω resistance when filled with the internal solution. The low electrode resistance and the small size of the acinar cells (6.4 ± 0.7 pF, $n = 16$) allowed fast cytosolic dialysis and a low access resistance (Marty and Neher, 1995). The bath chamber (~ 300 μl) was grounded using an Ag-AgCl pellet through a 1-M CsCl agar bridge. Liquid junction potentials between pipette and bathing solutions were experimentally determined to be +6.5 mV. Membrane potentials were corrected for this value. Pipette and cell membrane capacitance transients were subtracted from the records by the amplifier circuitry before sampling. Whole-cell Cl^- currents were recorded using an Axopatch 1-D amplifier (Axon Instruments, Inc., Foster City, CA). Digital-to-analog and analog-to-digital converters (12 bits) were used to generate the stimuli protocol and to sample the signals. Membrane potential was changed from -106 to $+94$ mV in 20-mV steps by delivering square pulses of 2.5-s duration every 10 s from a holding potential of -56 mV. Except where indicated, currents were filtered at 500 Hz using an 8-db/decade low-pass Bessel filter and sampled at 100 Hz using custom design software.

Solutions

The Ca^{2+} -buffered pipette solutions containing free $[\text{Ca}^{2+}]$ near 0 (<1 nM) up to 5 μM were prepared as described by Tsien and Pozzan (1989). EGTA and *N*-(2-hydroxyethyl)ethylenedinitrilo-*N,N',N'*-triacetic acid (HEDTA) were selected as high and low affinity Ca^{2+} buffers (K_d s of 95 nM and 3.5 μM , respectively). Consequently, they are suitable for preparing Ca^{2+} buffers in the nano- and micromolar range, respectively. The total concentration of these buffers was 20–48.6 mM (see Table I for specific concentrations). This ensured a high buffer capacity to overcome the cell's intrinsic Ca^{2+} buffering. The pH of the pipette solutions was set to 7.3 with 50 mM of *N*-tris(hydroxymethyl)methyl-2-aminoethanesulphonic acid (TES). High concentrations of Ca^{2+} and pH buffers assured control of both Ca^{2+} and pH during the course of these experiments. Monovalent cations were substituted with tetraethylammonium (TEA) in both the internal and external solutions to avoid contamination of the Cl^- currents by cation currents through nonselective or Ca^{2+} -activated K^+ channels. The $[\text{Cl}^-]$ in all internal (pipette) solutions was 47 mM. The tonicity of the internal solutions was 40 mosm kg^{-1} more hypotonic than the external solution to abolish the activation of the swelling-activated Cl^- channels present in these cells (Arreola et al., 1995b, 1996). Recordings were started after more than 4 min of dialysis to allow for the equilibration of the cytosolic contents with the pipette solution (Evans and Marty, 1986).

The standard external solution (326 mosm kg^{-1}) had the following composition (in mM): 135 TEA-Cl, 0.5 CaCl_2 , 20 TES, 45 D-mannitol, pH 7.3.

In many previous investigations of Ca^{2+} -activated Cl^- channels (Anderson and Welsh, 1991; Worrell and Frizzell, 1991; Park and Brown, 1995), monovalent cations were replaced with *N*-methyl-D-glucamine (NMDG). We found that the Ca^{2+} -activated Cl^- channel current in rat parotid acinar cells was larger with TEA compared with NMDG. An example of currents recorded with internal NMDG and with both NMDG and TEA in the bath solution is illustrated in Fig. 1. Shown in each panel are currents recorded (with 250 nM free Ca^{2+} in the pipette solution) at $+33$ (solid line) and -107 mV (dotted line) from a holding potential of -57 mV. In the upper panel the bath monovalent cation was NMDG and the usual time- and voltage-dependent Ca^{2+} -activated Cl^- currents are apparent (Arreola et al., 1995a, 1996; see also below). As apparent from this and the next two panels, there was a small, reversible increase in the current when TEA replaced NMDG as the major external cation.

Even though the currents were somewhat larger with TEA, there was no apparent change in current kinetics, as illustrated in the bottom panel. Here, the currents in the presence of NMDG at both potentials were scaled by a constant factor of 1.32. The scaled currents in NMDG are not distinguishable from those recorded with external TEA, including the tail currents recorded upon repolarization to -57 mV. These results not only demon-

TABLE I
Composition of Internal Solutions (in mM)

$[\text{Ca}^{2+}]$	TEA-Cl	CaCl_2	Ca-gluconate	EGTA-TEA	HEDTA-TEA	TEA-F	TES	D-mannitol	EGTA-NMDG
$<10^{-6}$	47	—	—	20	—	5	50	64	—
25×10^{-6}	37	5.241	—	25.241	—	5	50	84.5	—
100×10^{-6}	5	20.961	—	40.96	—	5	50	—	—
250×10^{-6}	—	23.5	2.705	36.205	—	5	50	—	—
10^{-3}	29.856	8.572	—	—	38.571	5	50	18	—
5×10^{-3}	—	23.5	5.076	—	48.571	5	50	—	—
250×10^{-6}	—	23.5	2.705	—	—	5	50	—	36.205

strate that there is no difference in channel gating kinetics, but they also show that the difference in current magnitude was independent of membrane potential.

We also compared internal TEA and NMDG as cation replacements. Although we did not directly compare these two cations on the same cell, the currents at all potentials were, in general, larger in the presence of TEA than NMDG—very similar to the results with external solutions. Also like the results with external solutions, there was no apparent difference in current kinetics. For example, the average activation time constant (e.g., see Fig. 10)

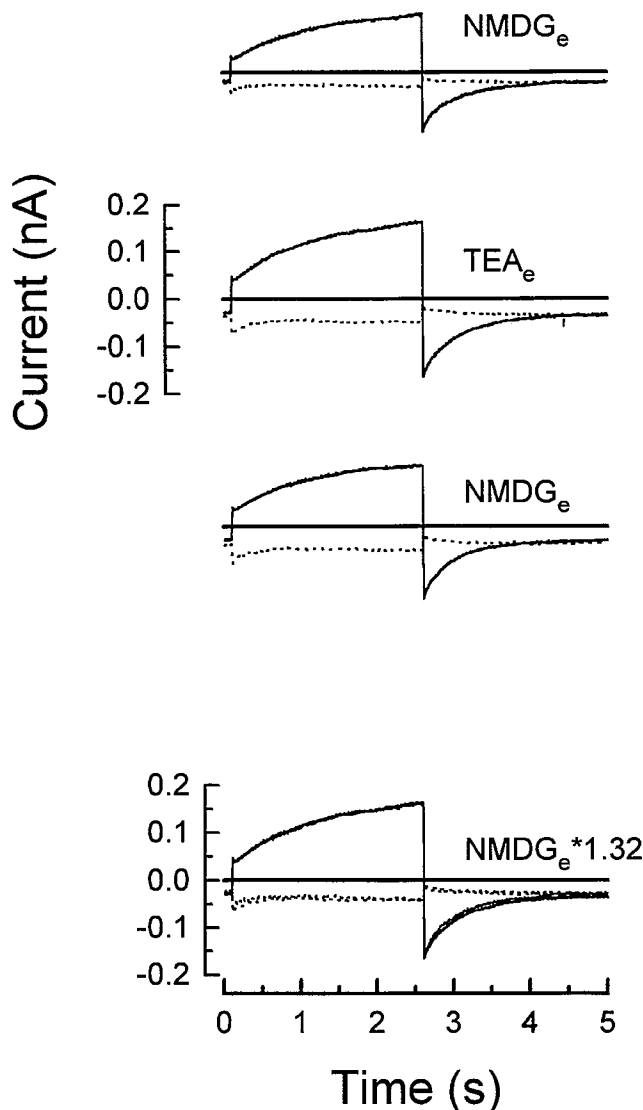


FIGURE 1. Ca^{2+} -dependent Cl^- currents in the presence of internal NMDG. Whole-cell currents recorded at +33 (continuous line) and -107 (dotted line) mV from a holding potential of -57 mV. A cell was dialyzed with a 250-nM free Ca^{2+} pipette solution containing NMDG as monovalent cation and sequentially perfused with NMDG- (top panel), TEA- (middle panel), then back to the NMDG-containing (lower panel) solution. The bottom portion of the figure shows Cl^- currents recorded in the presence of external TEA along with currents recorded in the presence of external NMDG (from the top panel above) scaled by a factor of 1.32. The NMDG external solution contained (in mM) 135 *N*-methyl-D-glucamine (NMDG)-Cl, 0.5 CaCl_2 , 20 TES, 45 D-mannitol, pH 7.3.

at +33 mV from four cells with internal and external NMDG was 786 ± 153 ms (SEM), and with internal and external TEA the value was 717 ± 77 ms ($n = 3$).

We do not know the mechanism for the smaller currents recorded in NMDG compared with TEA. Although TEA has been shown to block a voltage-activated Cl^- channel from brain cortex (Sanchez and Blatz, 1992), it does not block the Ca^{2+} -activated Cl^- currents we describe here. The currents were larger with TEA but there was no other voltage- or time-dependent effect. For these reasons we have chosen to use TEA as the major cation in our internal and external solutions.

Chemicals

EGTA, HEDTA, CaCl_2 , and TEA-Cl were from Fluka Chemie AG (Buchs, Switzerland). TES, D-mannitol, TEAF, $\text{Ca}(\text{gluconate})_2$, and other inorganic salts were obtained from Sigma Chemical Co. or Fluka Chemie AG. EGTA-TEA and HEDTA-TEA were made by mixing equimolar concentrations of EGTA or HEDTA with TEA-OH, and the pH was adjusted to 7.

Analysis

Steady-state current-voltage relations were constructed using the absolute amplitude of the currents at the end of the 2.5-s test pulse. These relationships were fit to a fourth-order polynomial, and the reversal potentials were obtained by extrapolation. Mean \pm SEM values are plotted or given. Positive currents reflect the inward flux of Cl^- and negative currents are outward Cl^- flux.

The relationship between average Cl^- current (I_{Cl}) (or conductance) and $[\text{Ca}^{2+}]_i$ at each membrane voltage was fit to the Hill equation:

$$y = \frac{y_{\text{max}}}{1 + \left(\frac{K_d}{[\text{Ca}]_i}\right)^{n_H}}, \quad (1)$$

where y is Cl^- channel current or conductance, y_{max} is the maximum current or conductance, K_d is the apparent dissociation constant, and n_H is the Hill coefficient. In the context of this equation, the Hill coefficient controls the steepness of the relation between Cl^- channel activation (current) and $[\text{Ca}^{2+}]_i$. It provides a lower limit on the number of Ca^{2+} ions required to activate the channels fully.

Whole-cell Cl^- conductance (g) was calculated in the usual manner as

$$g = \frac{I_{\text{Cl}}}{E_m - E_r}, \quad (2)$$

where E_m is the membrane voltage and E_r is the current reversal potential. Conductance-voltage relationships were fit to a Boltzmann distribution function:

$$g = \frac{g_{\text{max}}}{1 + \exp\left[\frac{(E_m - E_{0.5})}{s}\right]} \quad (3)$$

where g_{max} is the maximum conductance, $E_{0.5}$ is the membrane voltage necessary to obtain 50% of the maximal conductance, and the parameter s controls the voltage sensitivity of the conductance.

RESULTS

Ca^{2+} -dependent Cl^- Currents

We investigated the behavior of Ca^{2+} -dependent Cl^- channels in rat parotid cells at different $[\text{Ca}^{2+}]_i$. Fig. 2 shows whole-cell current records obtained at -106-

(*continuous lines*) and +94-mV (*dashed lines*) membrane potentials from five different cells dialyzed with internal solutions containing <1, 25, 100, 250, and 1,000 nM free Ca^{2+} . The macroscopic currents were negligible with <1 nM $[\text{Ca}^{2+}]_i$ and very small with 25 nM $[\text{Ca}^{2+}]_i$. Increasing the $[\text{Ca}^{2+}]_i$ to 100 or 250 nM induced the appearance of a current at -106 mV with an instantaneous component followed by a slower decay. The current recorded at +94 mV also had an instantaneous component but was followed by a large, slowly developing current. Upon repolarization to the holding potential of -56 mV from the +94-mV depolarization, a large inward tail current was recorded.

Increasing the $[\text{Ca}^{2+}]_i$ to 1,000 nM induced a further increase of both the holding and the steady-state currents as well as a large change in the time course of the whole-cell current. The current during a -106-mV test pulse showed an instantaneous increase followed by a very slow decay. In contrast, at +94 mV, the current ac-

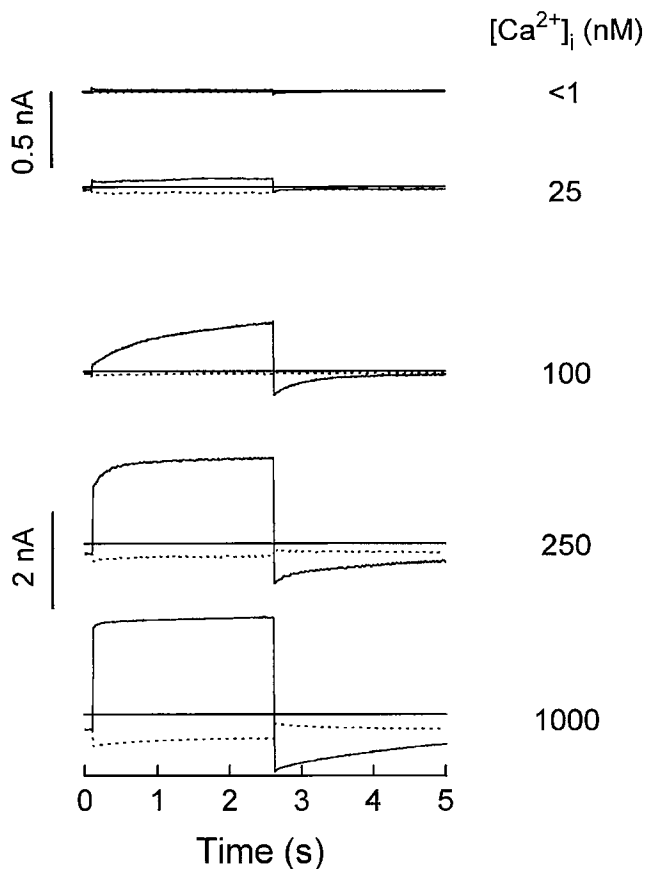


FIGURE 2. Ca^{2+} -dependent Cl^- currents from rat parotid acinar cells. Whole-cell currents recorded from five different cells dialyzed with pipette solutions containing (from top to bottom) <1, 25, 100, 250, and 1,000 nM free Ca^{2+} . Currents were obtained at membrane potentials of +94 (*continuous traces*) and -106 mV (*dashed traces*). The 0.5-nA calibration bar is associated with the records obtained with <1 and 25 nM $[\text{Ca}^{2+}]_i$. The 2-nA calibration bar is associated with the other records. Horizontal lines are 0 current level.

tivated very rapidly during the pulse. This was followed by a large, slow tail current during repolarization. These results show that increasing the levels of $[\text{Ca}^{2+}]_i$ caused the appearance of currents with increasing magnitude and with kinetics that were a function of $[\text{Ca}^{2+}]_i$. The time course of the currents recorded at different $[\text{Ca}^{2+}]_i$ are similar to those previously reported in rat parotid, sublingual, and lacrimal acinar cells (Evans and Marty, 1986; Arreola et al., 1995*a, b*, 1996; Zhang et al., 1995).

Fig. 3 shows a summary of the steady-state current-voltage relationships obtained from cells dialyzed with <1 (A), 25 (B), 100 (C), or 1,000 (D) nM free Ca^{2+} . The amplitude of the average current increased at all potentials as the $[\text{Ca}^{2+}]_i$ increased, especially for 100 nM and above (note scale change in parts C and D of this figure). The reversal potentials were -4 ± 7 mV (A), -22.4 ± 2.3 mV (B), -23.1 ± 1.4 mV (C), and -21.8 ± 3.7 mV (D). The average current recorded with <1 nM $[\text{Ca}^{2+}]_i$ serves as an estimate of the Ca^{2+} -insensitive current.

Except for the reversal potential obtained with <1 nM free $[\text{Ca}^{2+}]_i$, these values were close to the Cl^- equilibrium potential (-21 mV) calculated with the Nernst equation. Additional experiments (not shown) showed that changing the external $[\text{Cl}^-]$ from 10 to 136 mM induced a -52 mV/decade shift of the current reversal potential, not far from the predicted -59 mV/decade change of the Cl^- equilibrium potential. These results indicate that Cl^- is the main ion carrying the Ca^{2+} -dependent current recorded from acinar cells.

The characteristic outward rectification of the Ca^{2+} -dependent Cl^- currents (Evans and Marty, 1986; Anderson and Welsh, 1991; Ishikawa and Cook, 1993) was seen with concentrations of $\text{Ca}^{2+} \geq 25$ nM. However, the amount of outward rectification was reduced at $[\text{Ca}^{2+}]_i \geq 1,000$ nM. For example, with 250 nM $[\text{Ca}^{2+}]_i$, the average current amplitudes at -86 and $+74$ mV were -0.37 ± 0.1 and $+1.84 \pm 0.33$ nA, respectively. With $5 \mu\text{M}$ $[\text{Ca}^{2+}]_i$, these values were -0.89 ± 0.2 and 1.84 ± 0.46 nA, respectively. Thus, Ca^{2+} -activated Cl^- current increased 2.4-fold at -106 mV by raising $[\text{Ca}^{2+}]_i$ to $5 \mu\text{M}$, whereas no change was observed at $+74$ mV.

The Ca^{2+} dependence of the macroscopic Cl^- currents at two membrane potentials is depicted in Fig. 4. Fig. 4 A shows steady-state average currents measured at -66 mV with the indicated $[\text{Ca}^{2+}]_i$. To provide a quantitative description of the Ca^{2+} dependence, we fit the Hill equation (Eq. 1) to these data (*solid line*) and obtained an apparent K_d of 300 nM and a Hill coefficient (n_H) of 1.2. The coefficient value is close to but larger than that expected (1.0) if a single Ca^{2+} ion were involved in Cl^- channel activation at this potential.

Fig. 4 B shows the average steady-state currents at

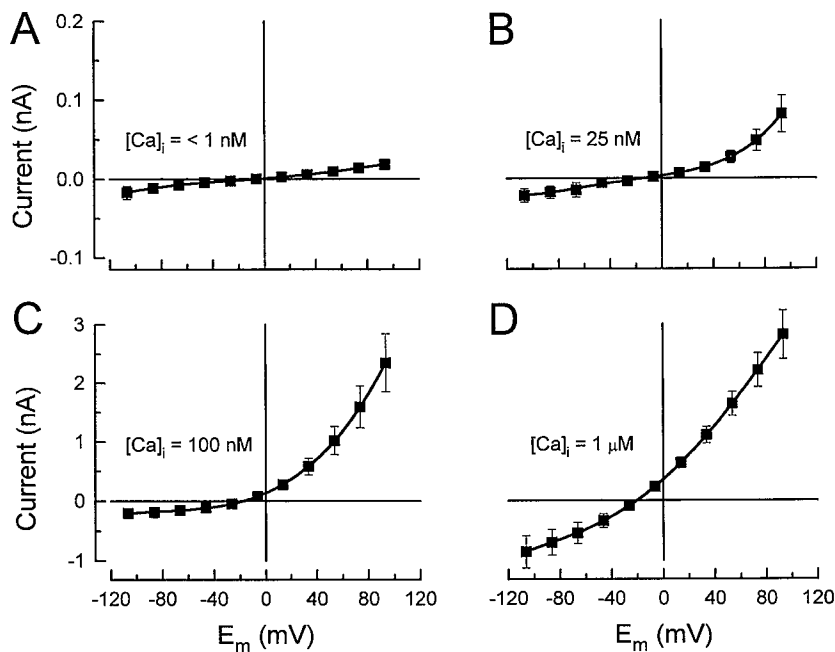


FIGURE 3. Steady-state current-voltage relationships at different $[Ca^{2+}]_i$. Current-voltage relations were constructed from currents recorded from cells dialyzed with <1 (A), 25 (B), 100 (C), and 1,000 (D) nM free Ca^{2+} . Mean currents at each potential were obtained by averaging the amplitude of the currents from 4 (A), 5 (B), 11 (C), and 4 (D) cells. Continuous lines are the fit of a fourth-order polynomial to data. Ordinate scales on A and C are also valid for B and D, respectively. The abscissa scale is the same for all plots.

+74 mV along with the fit of the Hill equation. The apparent K_d at +74 mV was 61 nM, fivefold smaller than the 300 nM value at -66 mV. Further, the current at this potential was a very steep function of $[Ca^{2+}]_i$, as indicated by the n_H value of 2.7. These results imply that the Ca^{2+} sensitivity of Cl^- channels was a function of membrane potential and suggest also that more than one Ca^{2+} ion was involved in the activation of Cl^- channels at positive potentials.

Voltage Dependence of Cl^- Channels

The current at any potential is a function of the number of channels present, the channel open probability, and the driving force moving the ions. The contribution of these variables can be separated if the number of channels is constant and the open channel current is a linear function of the membrane potential and consequently of the driving force. An analysis of the voltage dependence of open Ca^{2+} -dependent Cl^- channel current at 250 nM $[Ca^{2+}]_i$ is illustrated in Fig. 5. The voltage protocol used to generate the currents is illustrated in Fig. 5 A. A 500-ms prepulse to +74 mV was used to open a constant number of channels, and the voltage dependence of the open channel current was assayed by the magnitude of the tail current generated by different repolarizing potentials ranging from -106 to +54 mV in 20-mV steps. Fig. 5 B shows the superimposed current records obtained with this protocol. The instantaneous current-voltage relation (Fig. 5 C) was constructed by plotting the amplitude of the tail current measured 4 ms after the prepulse end against the repolarizing potential.

The results of Fig. 5 C show that the instantaneous

current-voltage relation of the Ca^{2+} -activated Cl^- channels in rat parotid cells is linear. However, the concentration gradient of Cl^- used in these experiments might, under certain circumstances, be expected to result in a rectification of the current at very positive and negative potentials (Goldman, 1943; Hodgkin and Katz, 1949). We do not know the reason for the apparent linearity, but the current rectification of many Cl^- channels does not, in general, follow the prediction of the Goldman-Hodgkin-Katz equation. These include Ca^{2+} -activated Cl^- channels in T84 cells (Anderson and

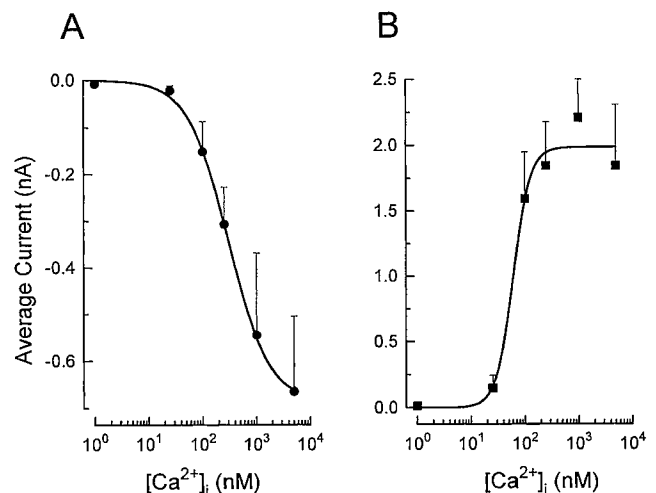


FIGURE 4. Concentration-response curves of the effect of Ca^{2+} on the macroscopic Cl^- currents. Mean current- $[Ca^{2+}]_i$ relationships at -66 mV (A) and +74 mV (B). Continuous lines are the fits of the Hill equation (Eq. 1) to the data with the following parameters: -66 mV: $K_d = 300$ nM and $n_H = 1.2$; +74 mV: $K_d = 61$ nM and $n_H = 2.7$. Data were obtained from $n = 4-16$ cells.

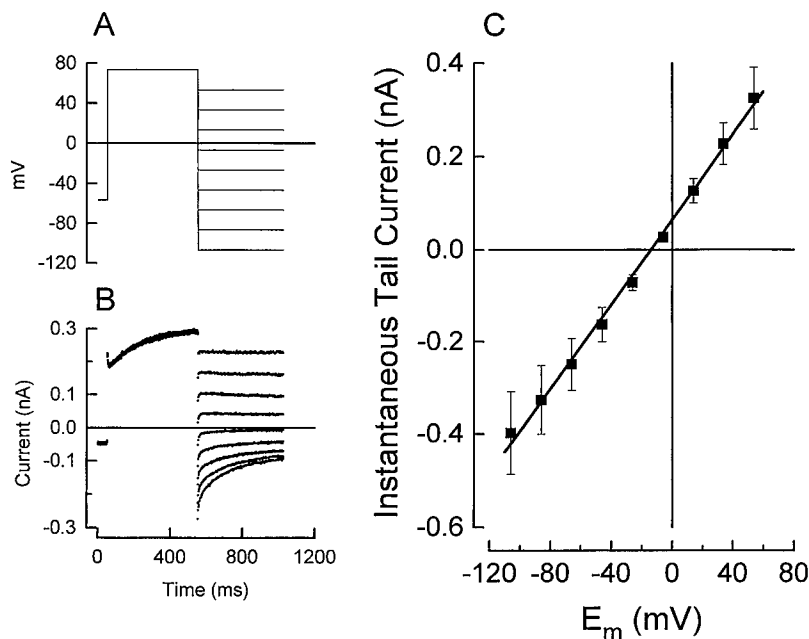


FIGURE 5. Instantaneous current–voltage relation of Ca²⁺-dependent Cl⁻ channels. (A) Voltage protocol used to generate the Cl⁻ tail currents. A 0.5-s prepulse potential to +74 mV was followed by repolarizing pulses to various potentials ranging from -106 to +54 mV in 20-mV steps. (B) Tail currents recorded from a cell dialyzed with 250 nM free Ca²⁺ using the protocol depicted in A. Data were sampled at 2-ms intervals. (C) Relationship between tail current amplitude and membrane potential. Line is a least-squares linear regression fit to tail currents measured 4 ms after repolarization ($n = 4$).

Welsh, 1991), Cl⁻ channels in cardiac cells (Overholt et al., 1993), and cloned, voltage-gated Cl⁻ channels (Pusch et al., 1995). Whatever the reason, the linearity of the instantaneous current–voltage relation means that conductance, computed from Eq. 2, can be used as a measure of channel open probability.

The voltage dependence of Cl⁻ channel conductance from three cells is illustrated in Fig. 6. The conductance–voltage relations (computed from Eq. 2) are shown for 100 (●), 250 (▲), and 1,000 nM Ca²⁺ (▼). The voltage dependence was sigmoid at all Ca²⁺ levels and was shifted to more hyperpolarized potentials as the [Ca²⁺]_i was increased. The sigmoid nature of the voltage dependence was described by a Boltzmann function (Eq. 3, lines). The Ca²⁺-dependent shift in the conductance was reflected in the $E_{0.5}$ values of +62, +4.3, and -38 mV at 100, 250, and 1,000 nM Ca²⁺, respectively. This result accounts for the changes in current rectification observed in Fig. 3 at high [Ca²⁺]_i. The maximum conductance (g_{max}) was little affected by intracellular Ca²⁺: g_{max} values obtained from the Boltzmann fits to data in Fig. 6 were 32, 32, and 33 nS at 100, 250, and 1,000 nM Ca²⁺, respectively. From a similar analysis of all the data (4–16 cells at each of five [Ca²⁺]_i levels), we estimate an average maximum conductance of 31.4 ± 0.05 nS. This value was used to compute the relative Cl⁻ channel conductance in our analysis of the Ca²⁺ dependence of channel activation.

Ca²⁺ Dependence of Cl⁻ Channels

As was shown previously (Fig. 5 and related text), the relative Cl⁻ conductance reflects the fraction of open channels and, consequently, is an index that can be used to estimate directly the Ca²⁺ dependence of Cl⁻

channel activation. The average relative conductances obtained for voltages between -106 and +74 mV at different [Ca²⁺]_i are shown in Fig. 7. To enhance the clarity of this figure, SE limits are not shown, but they are similar to those of Fig. 8. The relative conductance was a function of both voltage and [Ca²⁺]_i. At a fixed Ca²⁺, the relative conductance increased with increased depolarization, whereas, at a fixed voltage, it gradually increased as the [Ca²⁺]_i increased. The relative conductance appeared to reach an asymptotic value for [Ca²⁺]_i near 5 μ M that depended on the membrane potential. This result suggests that Ca²⁺ alone was not sufficient to induce full channel activation; rather, a combination of Ca²⁺ and voltage was required. The relative conductance data were fit to the Hill equation (Fig. 7, *contin-*

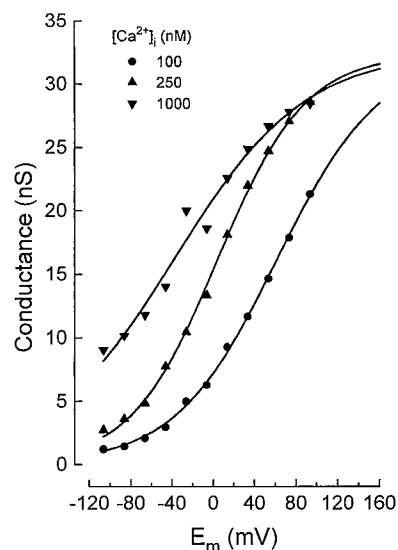


FIGURE 6. Voltage dependence of Ca²⁺-dependent Cl⁻ channel conductance from rat parotid acinar cells. Whole-cell conductance–voltage relations from cells dialyzed with 100 (●), 250 (▲), and 1,000 (▼) nM free Ca²⁺. Lines are the fits of Boltzmann function (Eq. 3) to data with the following parameters: 100 nM Ca²⁺: $g_{max} = 32.4$ nS, $E_{0.5} = +62$ mV, $s = 50$ mV; 250 nM Ca²⁺: $g_{max} = 32.3$ nS, $E_{0.5} = +4.3$ mV, $s = 42$ mV; and 1,000 nM Ca²⁺: $g_{max} = 32.5$ nS, $E_{0.5} = -38$ mV, $s = 63$ mV.

ous lines) to obtain the apparent dissociation constant (K_d) and the Hill coefficient (n_H) at different membrane potentials.

Details of the fitting of the Hill equation to channel activation data can be seen in the examples depicted in Fig. 8. The average relative conductance at -66 mV is shown in Fig. 8 A along with the Hill equation fit (solid line). The best-fit values of the K_d and n_H were 360 nM and 1.2—similar to the values obtained by fits to membrane current (Fig. 4 A). The average relative conductance data at $+74$ mV were fit by values of 73 nM and 2.3 for K_d and n_H , respectively. The data at -66 mV were reasonably well fit by the Hill equation constrained to have a coefficient of 1.0 (dashed line) but provided a poor description to the data at $+74$ mV (Fig. 8 B, dashed line), supporting the conclusion from Fig. 4 B that more than one Ca^{2+} ion is required for channel activation. In addition, the Ca^{2+} sensitivity, as judged by both the apparent K_d and the Hill coefficient, was a function of membrane voltage.

A summary of the voltage dependence of K_d and n_H is presented in Fig. 9. These parameters were obtained from the fits shown in Fig. 7. Fig. 9 A shows the relationship between the apparent K_d and membrane voltage. The K_d decreased with increased depolarization in an approximately linear fashion in the semilogarithmic plot of Fig. 9 A, and so these K_d values could be fit (line) by the following equation:

$$K_d(E_m) = K_d^0 \exp\left(\frac{-\delta FE_m}{RT}\right), \quad (4)$$

where K_d^0 is the dissociation constant at an E_m value of 0 mV. The parameter, δ , controls the voltage sensitivity,

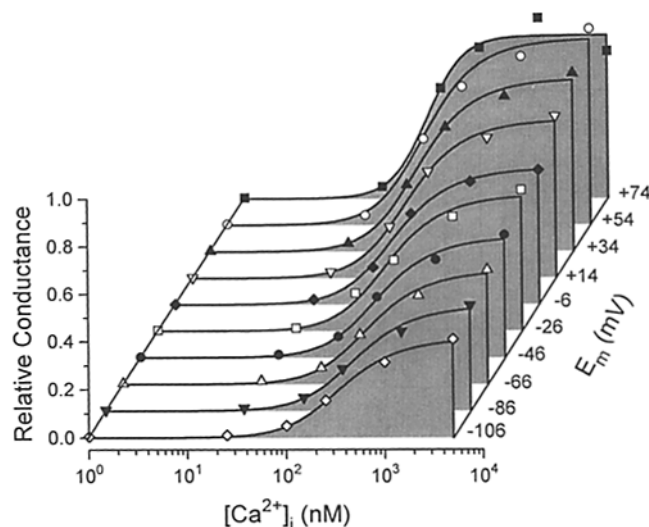


FIGURE 7. Activation of Ca^{2+} -dependent Cl^- channels by Ca^{2+} and voltage. Mean relative conductance without SE are plotted. Relative conductance was obtained by dividing the absolute conductance by the average maximum conductance (31 nS). Membrane potential was changed from -106 to $+74$ mV in 20-mV steps. Continuous lines are the Hill equation fits to data.

and its interpretation will be discussed below. R , T , and F have their usual thermodynamic meanings. The best fit of this equation to the K_d data of Fig. 9 A was with K_d^0 and δ values of 183 nM and 0.13, respectively.

Fig. 9 B summarizes the voltage dependence of n_H . At all potentials, this parameter was >1.0 , the value expected if a single Ca^{2+} ion were involved in channel activation. The values at negative voltages were not much larger than 1.0, but n_H increased with membrane depolarization to values as large as 2.5.

Kinetics of Ca^{2+} -dependent Cl^- Currents

The activation kinetics of Ca^{2+} -dependent Cl^- channels were evaluated at different $[\text{Ca}^{2+}]_i$. A single exponential time function was fit to the current as has been done previously for Ca^{2+} -dependent Cl^- currents from rat lacrimal and sheep parotid acinar cells (Evans and Marty, 1986; Ishikawa and Cook, 1993). The inset in Fig. 10 depicts an example of the fit of raw currents at $+94$ mV obtained from a cell dialyzed with 250 nM $[\text{Ca}^{2+}]_i$ and held at -56 mV. Most of the time course of the current was described by a single-exponential time function with a time constant of 0.22 s (solid line). However, there was an additional slow component apparent near the end of the 2.5-s pulse. Since the relative contribution of the slow component to the total current was rather small, it was ignored in the analysis. The plot in Fig. 10 shows the time constant of the macroscopic currents obtained from the fits at $+94$ (■), $+74$ (□), and -86 mV (●) obtained from cells dialyzed with different $[\text{Ca}^{2+}]_i$. This plot shows that the rate of activation of Ca^{2+} -dependent Cl^- channels was increased with in-

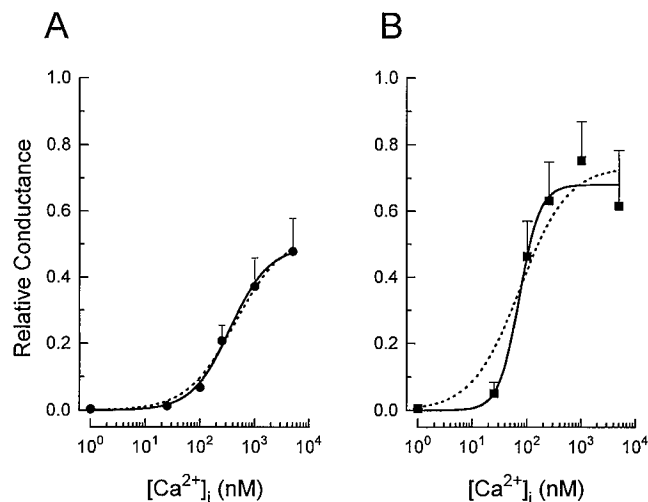


FIGURE 8. Ca^{2+} dependence of Cl^- channel activation. Relative conductance as a function of $[\text{Ca}^{2+}]_i$ at -66 mV (A) and $+74$ mV (B). Continuous lines are the fits of the Hill equation to data with the following parameters: -66 mV: $K_d = 360$ nM and $n_H = 1.2$; $+74$ mV: $K_d = 73$ nM and $n_H = 2.3$. Broken lines represent the fit of the Hill equation using a fixed value of $n_H = 1$. Data points are mean values from 4–16 cells.

creased internal $[Ca^{2+}]_i$. This also indicates that, at a fixed Ca^{2+} concentration, there was little, if any, consistent change in the current time constant over a 180-mV range of membrane voltage.

A Model for Activation of Ca^{2+} -dependent Cl^- Channels

Although we did not design this study to provide data to test possible models of Ca^{2+} -dependent activation of the Cl^- channels, our results, nevertheless, have implications for possible mechanistic schemes. Only models that require more than a single Ca^{2+} ion for channel activation will be consistent with the finding of n_H values larger than one. Models with simultaneous binding of two Ca^{2+} ions will exhibit a fixed value of n_H of two and are, therefore, inconsistent with the results of Fig. 9 B. Thus, models with sequential Ca^{2+} binding steps must be considered.

Any model with a Ca^{2+} binding step as the last transition before channel opening predicts maximal activation at all potentials with saturating Ca^{2+} concentrations. The data of Fig. 7 show that this is not the case for Ca^{2+} -activated Cl^- channels in rat parotid acinar cells. Thus, we consider a model with two sequential Ca^{2+} binding steps followed by a transition to an open state. Scheme I represents this model with the binding of two Ca^{2+} ions to two independent sites with identical affinity.

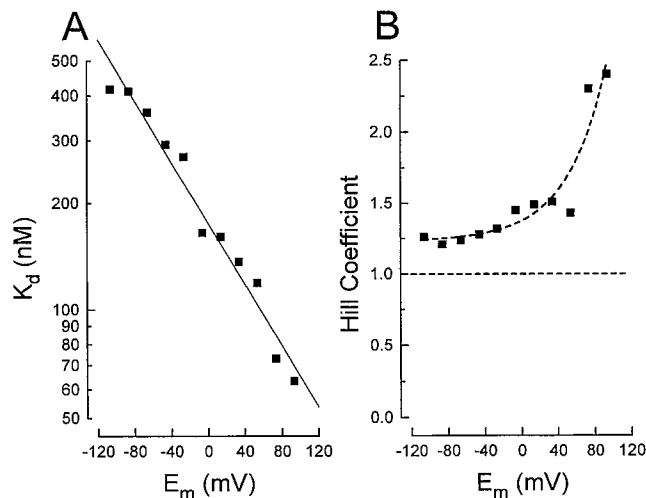
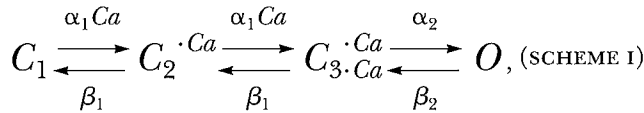


FIGURE 9. Voltage dependence of the apparent K_d and Hill coefficient. (A) Values of K_d at different membrane voltages obtained from fits of the Hill equation to data as in Fig. 7. The line represents the fit of Eq. 4 to the data with the following parameters: $K_d^0 = 183$ nM and $\delta = 0.13$. (B) Voltage dependence of the Hill coefficient, n_H . The line is the fit of an exponential function and has no theoretical significance.

where C and O represent closed and open (conducting) channel conformations, respectively, α_1 and β_1 represent the rate constants of the Ca^{2+} -dependent steps, and α_2 and β_2 the forward and backward rate constants of the final transition to the open state. In general, any or all of the rate constants could be voltage dependent. Such a multistep model predicts multi-exponential kinetics, but the currents (e.g., Fig. 2) appear to contain an instantaneous component followed by a single-exponential relaxation to steady state (but see Fig. 10, *inset*). We consider both components to be associated with the same class of Ca^{2+} -activated Cl^- channels. We further consider the instantaneous component to be due to very fast Ca^{2+} binding kinetics and,

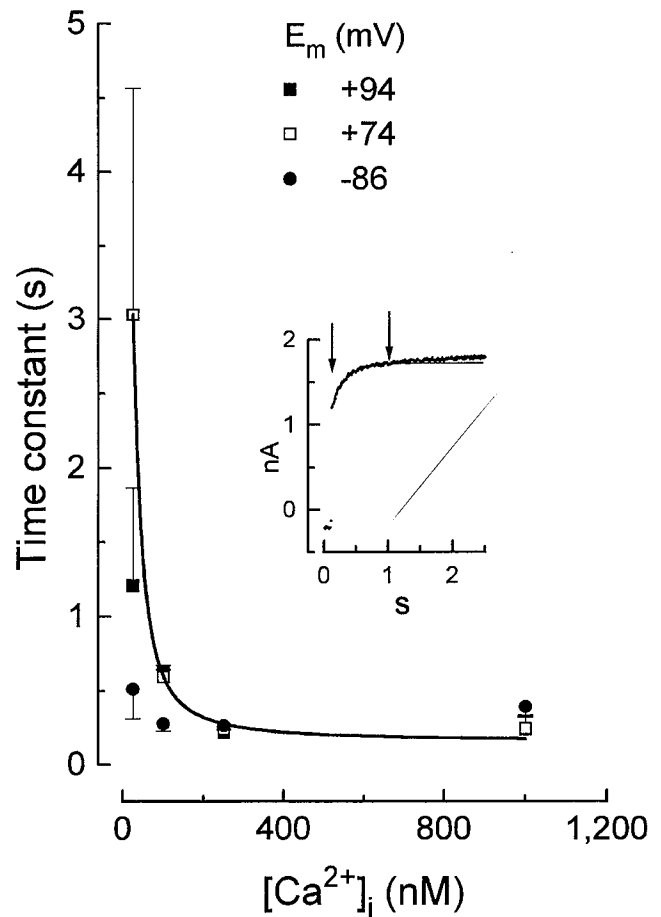


FIGURE 10. Kinetics of Ca^{2+} -dependent Cl^- currents at different $[Ca^{2+}]_i$. (*Inset*) An example of a single-exponential fit (*continuous line*) used to obtain the time constant of current activation at +94 mV from a cell dialyzed with 250 nM $[Ca^{2+}]_i$. Arrows indicate the beginning and end of the current data (*dots*) used in the fitting procedure. This current trace was best fit with a time constant value of 0.22 s. The rest of the figure shows mean time constant values obtained at +94 (■), +74 (□), and -86 mV (●) from cells dialyzed with 25, 100, 250, and 1,000 nM free $[Ca^{2+}]_i$ ($n = 4, 10, 10$, and 4, respectively). The continuous line is the fit of Eq. 8 to data obtained at +74 mV used to estimate the forward rate constant α_2 of Scheme I.

in the context of the model, the first two kinetic steps to be in equilibrium.

The steady-state open probability for this model is given by

$$P_o = \frac{1}{1 + K_2 \left(\frac{K_1^2}{Ca^2} + \frac{K_1}{Ca} + 1 \right)}, \quad (5)$$

where K_1 and K_2 are the equilibrium constants of the transitions and are equal to β_1/α_1 and β_2/α_2 , respectively. This model predicts that P_o at any potential is equal to $(1 + K_2)^{-1}$ for saturating levels of Ca^{2+} . This is consistent with the data of Fig. 7 and the graded increase in conductance (at saturating $[Ca^{2+}]_i$) with membrane voltage attributed to a voltage dependence of the equilibrium constant K_2 .

Examples of fits of this model to steady-state channel activation data are illustrated in Fig. 11. Shown in this figure is the Ca^{2+} dependence of relative conductance at +54 (■) and -66 mV (●). Also shown are fits of Eq. 5 to these data with K_1 and K_2 as adjustable free parameters. The model is seen to provide a reasonable description of the Ca^{2+} dependence of activation over a large voltage range. From the fit to the data at -66 mV, we obtained values of 300 nM and 1.1 for K_1 and K_2 , respectively; at +54 mV these values were 180 nM and 0.28. These findings indicate a voltage dependence of both K_1 and K_2 model parameters.

Fig. 12 provides a summary of the voltage dependence of K_1 (A) and K_2 (B) obtained from fitting the model to data like those shown in Fig. 11. K_1 decreased from 310 to 140 nM over the voltage range from -106 to +94 mV. Since K_1 is the equilibrium constant for each Ca^{2+} binding step, it may be somewhat comparable to the K_d value obtained from the Hill equation fits (Fig. 9 A). Indeed, a comparison of Figs. 12 A and 9 A reveals the general similarity of these two parameters.

K_2 describes the equilibrium of the last (Ca^{2+} -independent) step before channel opening. As can be seen

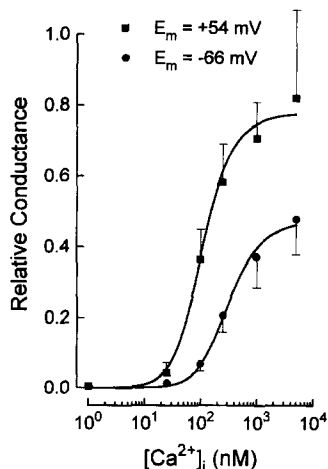


FIGURE 11. Ca^{2+} -dependent Cl^- channel activation and a simple kinetic model. Relative conductance at +54 (■) and -66 mV (●) were obtained as described in Fig. 7. Continuous lines are the fits of Eq. 5 to the data. From the fits to the -66-mV data, K_1 and K_2 values of 300 nM and 1.1 were obtained. Fits to +54 mV data yielded values of 180 nM and 0.28, respectively. Data were collected from five or more cells.

in Fig. 12 B, this equilibrium constant, like K_1 , decreased with membrane depolarization. However, since K_2 was more voltage sensitive than K_1 , it appears that most of the voltage dependence of channel activation would be associated with channel opening step.

Since both K_1 and K_2 appear to be linearly related to membrane voltage in the semilogarithmic plot of Fig. 12, A and B, we fit an exponential function to these data (analogous to Eq. 4). The lines in these figures are the results of such fits and provide the following empirical description of these two model parameters:

$$K_1(E_m) = 214 \exp\left(\frac{0.13FE_m}{RT}\right) \text{ nM}$$

$$K_2(E_m) = 0.58 \exp\left(\frac{0.24FE_m}{RT}\right). \quad (6)$$

Examples of the ability of the model in Scheme I to simulate the voltage and Ca^{2+} dependence of channel conductance and current are illustrated in Fig. 13. A contains average relative conductance-voltage relations from cells dialyzed with 100 (●, $n = 10$) and 250 (■, $n =$

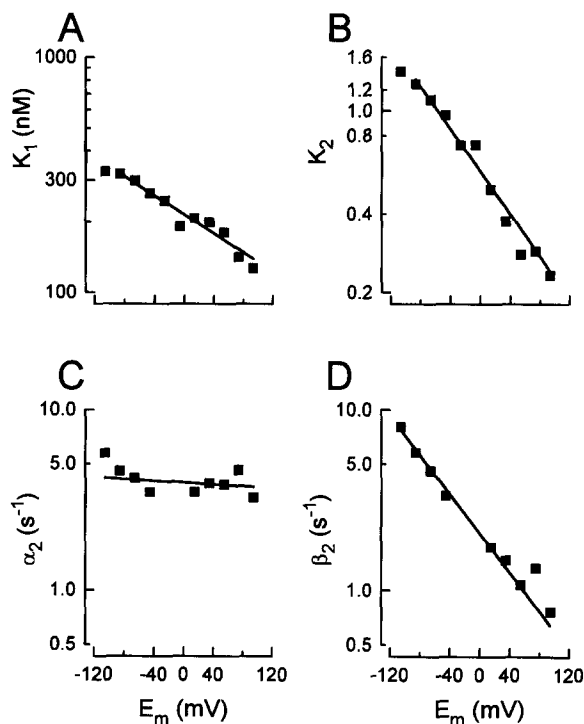


FIGURE 12. Voltage dependence of the equilibrium constants K_1 and K_2 and of the rate constants α_2 and β_2 . K_1 (A) and K_2 (B) at different membrane potentials were obtained from fits like those shown in Fig. 11. Continuous lines are the fit of an exponential voltage function to the data; the fitted parameters are shown in Eq. 6. α_2 (C) and β_2 (D) were calculated by using Eq. 8 as described in the text and $K_2\alpha_2$, respectively. The continuous line through α_2 values is a linear regression with a slope of $-0.0022 \text{ s}^{-1}\text{mV}^{-1}$. The continuous line through β_2 is a fit of an exponential function similar to Eq. 4 with the following parameters: $\beta_2(0) = 2.07 \text{ s}^{-1}$ and $\delta = 0.32$.

18) nM free Ca^{2+} . The solid lines are the results of computations with Eq. 5 using the K_1 and K_2 values from Eq. 6 and provide reasonable descriptions of the experimental data.

Fig. 12 B is a plot of the transformation of the conductance–voltage data to illustrate that the rectification of the current–voltage relationship and the Ca^{2+} -dependent change in outward rectification was reproduced by the model. The 100 nM data (●) in this figure are reproduced from Fig. 3 C along with experimental data (■) obtained with 250 nM Ca^{2+} . The hyperpolarizing shift of the conductance–voltage relation with increased Ca^{2+} apparent in Fig. 12 A results in the reduced outward rectification of the channel current shown in Fig. 12 B. Since the model provided a description of channel conductance, it also reproduced the steady-state current–voltage relation (*lines*).

Since the model of Scheme I provided a good simulation of the steady-state properties of the Ca^{2+} -activated Cl^- channels, it was reasonable to investigate its ability to reproduce kinetic data as well. The time-dependent open probability of the model channel is given by

$$P_o(t) = P_o(\infty) - [P_o(\infty) - P_o(0)] \exp\left(\frac{-t}{\tau}\right), \quad (7)$$

where $P_o(0)$ and $P_o(\infty)$ are the open probability at time $t = 0$ and ∞ , respectively. Since fits of the model to steady-state data have produced estimates for the equilibrium constants, K_1 and K_2 , it was useful to express the time constant, τ , in terms of these parameters:

$$\frac{1}{\tau} = \frac{\alpha_2}{\frac{K_1^2}{Ca^2} + \frac{K_1}{Ca} + 1} + \alpha_2 K_2 \quad (8)$$

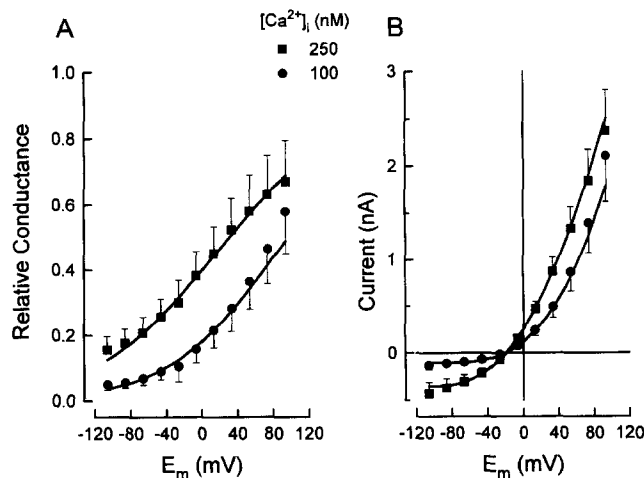


FIGURE 13. Model simulation of the steady-state properties of Ca^{2+} -dependent Cl^- channels. Relative conductances (A) and steady-state current–voltage relations (B) at 100 (●, $n = 10$) and 250 nM $[\text{Ca}^{2+}]_i$ (■, $n = 18$) are described by the three-step kinetic model (*continuous lines*). Model computations are P_o from Eq. 5 with K_1 and K_2 values given by Eq. 6. Model currents computed as $P_o(E_m - E_{\text{Cl}})g_{\text{max}}$ with $g_{\text{max}} = 31$ nS.

where α_2 is the forward rate constant for the last Ca^{2+} -independent step in Scheme I. Estimates for α_2 values, along with values of K_1 and K_2 from Eq. 6, allow prediction of channel kinetics through Eq. 7. We obtained values for α_2 by fitting Eq. 8 to time-constant data like those illustrated in Fig. 10. The line in that figure is the result of fitting Eq. 8 to the data at +74 mV. From this and other similar procedures, we obtained the α_2 values plotted in Fig. 12 C. Over the voltage range of -106 to $+94$ mV, α_2 values were between 3.3 and 5.7 s^{-1} with no consistent voltage dependence, indicating that the transition from the last closed state to the open state in the model (Scheme I) has little or no voltage dependence. But since K_2 (which is equal to β_2/α_2) is voltage dependent, the reverse rate constant β_2 must, likewise, be voltage dependent. Fig. 12 D shows the voltage dependence of β_2 determined as $\alpha_2 K_2$. Over the voltage range of -106 to $+94$ mV, β_2 values changed between 8 and 0.7 s^{-1} in an approximately linear relation in the semilogarithmic plot.

Examples of the simulation of channel kinetics by the model of Scheme I are shown in Fig. 14 (*right*) along with average currents (*left*) obtained from 7, 13, and 4 cells dialyzed with 100, 250, and 1,000 nM Ca^{2+} , respectively. The time course of current activation at -106 (*solid lines*) and $+94$ mV (*dashed lines*) are illustrated. For these simulations, K_1 and K_2 values from Eq. 5 were

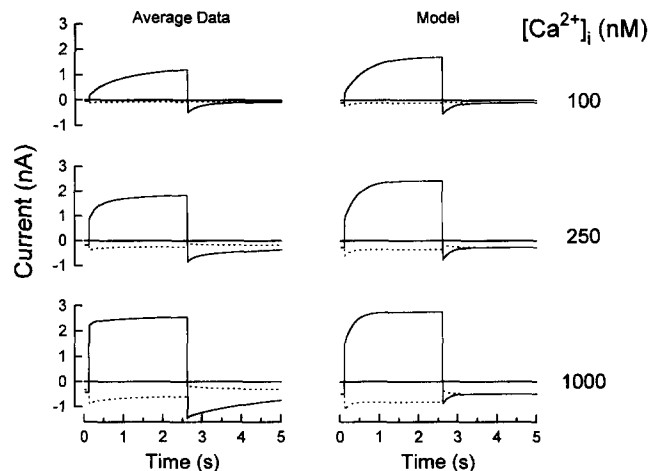


FIGURE 14. Model simulation of the kinetic properties of Ca^{2+} -dependent Cl^- channels. (*Left*) Average current data obtained from 7, 13, and 4 cells dialyzed with 100, 250, and 1,000 nM Ca^{2+} , respectively. Currents were obtained at membrane potentials of $+94$ (*continuous traces*) and -106 mV (*dashed traces*). (*Right*) Model simulations for the conditions as in the left panel. Model currents were computed from P_o (Eq. 7) as in Fig. 13 B. $P_o(0)$ (at the holding potential of -56 mV) and $P_o(\infty)$ (at the test potentials of -106 or $+94$ mV) at each $[\text{Ca}^{2+}]_i$ were calculated from Eq. 5 with the model K_1 and K_2 values (see Figs. 12, A and B, Eq. 6, and associated text). Time constant values were from Eq. 8 with K_1 and K_2 values as above and a constant value of 3.84 s^{-1} for α_2 (Fig. 12 C and associated text).

used along with a constant value of α_2 near 4 s^{-1} (see Fig. 12 C).

The model was able to provide a reasonable simulation of activation kinetics of macroscopic Cl^- currents during the voltage clamp step at different Ca^{2+} concentrations. It also reproduced reasonably well the Ca^{2+} -dependent change in the relative amount of instantaneous and time-dependent components. The model did not, however, reproduce the very slow tail currents that follow the voltage clamp steps to $+94 \text{ mV}$ in $1,000 \text{ nM Ca}^{2+}$.

DISCUSSION

Summary of Findings

Our results demonstrate that the activation of Ca^{2+} -activated Cl^- channels in rat parotid acinar cells depends on both membrane voltage and $[\text{Ca}^{2+}]_i$. Membrane voltage was insufficient to activate Cl^- channels in the absence of internal Ca^{2+} . Cl^- current was activated at $[\text{Ca}^{2+}]_i$ between 25 and $5,000 \text{ nM}$. The K_d from the Hill equation was voltage dependent and ranged from $\sim 400 \text{ nM}$ at negative potentials (near -100 mV) to $\sim 50 \text{ nM}$ at positive potentials ($+94 \text{ mV}$). In addition, the sensitivity of the Cl^- channel to intracellular Ca^{2+} , as judged by the Hill coefficient, n_H , was increased at depolarized potentials. The time course of current activation had both an instantaneous and a time-dependent component. The time dependence was reasonably well described by a single-exponential function with a time constant near 3 s at 25 nM Ca^{2+} and decreased to 0.2 s at high $[\text{Ca}^{2+}]_i$ ($1,000 \text{ nM}$). The kinetics of Cl^- channel activation as shown by the time constant had little or no voltage sensitivity.

Comparison to Other Ca^{2+} -dependent Cl^- Channels

The current-voltage relationship described here has the same outward rectification as the Ca^{2+} -dependent Cl^- channels in other secretory epithelial cells (Evans and Marty, 1986; Cliff and Frizzell, 1990; Anderson and Welsh, 1991; Ishikawa and Cook, 1993). The activation kinetics of the Ca^{2+} -dependent Cl^- current in rat parotid acinar cells was similar also to the time course of the Ca^{2+} -dependent Cl^- currents previously described in rat lacrimal gland, sheep parotid gland, T84 cells, and hepatocytes (Evans and Marty, 1986; Cliff and Frizzell, 1990; Anderson and Welsh, 1991; Ishikawa and Cook, 1993; Koumi et al., 1994). A single-exponential process dominated the activation of Ca^{2+} -dependent Cl^- channels in rat parotid acinar cells with little or no voltage dependence. An equivalent behavior has been reported in lacrimal and sheep parotid cells (Evans and Marty, 1986; Ishikawa and Cook, 1993).

Our results demonstrated that the Ca^{2+} -dependent Cl^- channels in rat parotid acinar cells are activated by

$[\text{Ca}^{2+}]_i > 25 \text{ nM}$. A similar $[\text{Ca}^{2+}]_i$ was required to activate Ca^{2+} -dependent Cl^- channels in sheep parotid acinar cells (Ishikawa and Cook, 1993). However, Cl^- channels from rat parotid acinar cells appeared to be more sensitive to Ca^{2+} than those channels expressed in lacrimal cells (Evans and Marty, 1986).

Activation Mechanism of Ca^{2+} -dependent Cl^- Channels

The Ca^{2+} affinity of the Cl^- channels from rat parotid acinar cells increased as the membrane potential became more positive. This increase in affinity was reflected as a decrease in the K_d from the Hill equation at depolarized potentials, and it was accompanied by an increase in n_H from 1.2 to 2.4, suggesting at least two Ca^{2+} ions are involved in channel activation.

Activation of parotid cell Cl^- channels by simultaneous binding of any fixed number of Ca^{2+} ions is inconsistent with our finding of a voltage-dependent Hill coefficient (Fig. 9 B). Also, any mechanism that includes a Ca^{2+} binding step as the last transition before channel opening (as in the model of Evans and Marty, 1986) is inconsistent with the data of Fig. 7. Such a mechanism would provide full activation at all potentials with saturating Ca^{2+} levels. The graded increase in activation with membrane voltage implies a final, voltage-dependent, Ca^{2+} -independent step before channel opening.

These mechanistic considerations are implemented in the model represented in Scheme I. In this model, each channel contains two identical Ca^{2+} binding sites, both of which must be occupied before the channel can undergo the final conformational change to the conducting state. As shown above, this very simple model is able to reproduce almost all of the major features of the parotid cell Cl^- channels.

The fit of this model to the data required a voltage-dependent equilibrium constant (K_1) for the interaction of Ca^{2+} with the channel. One interpretation of this result is that Ca^{2+} ions bind to a site within the membrane electric field. An estimate of the location of the Ca^{2+} binding site can be determined from the voltage sensitivity of K_1 (Woodhull, 1973). The line in Fig. 12 A is a reasonable description of the voltage dependence of K_1 and is equivalent to the binding of Ca^{2+} to a site 13% into the membrane field from the cytoplasmic surface.

The voltage dependence of Ca^{2+} sensitivity could, alternatively, be explained by voltage-independent binding of Ca^{2+} to a channel conformation that itself is voltage dependent. Although our present data cannot eliminate this possibility, such a mechanism requires at least one channel conformation in addition to those of Scheme I.

As described in Results, the major features of the Ca^{2+} -activated Cl^- channels in parotid acinar cells were

reproduced by the simple model represented in Scheme I. These include a quantitatively accurate description of the steady-state properties (e.g., Figs. 11 and 13) and a reasonable, qualitative reproduction of the current kinetics (Fig. 14). The model did not provide a quantitatively accurate description for several properties at 1,000 nM Ca^{2+} : (a) the activation kinetics at positive potentials (e.g., +94 mV in Fig. 14) were rather slower than the data; (b) the relative amount of time-dependent current at positive potentials (e.g., +94 mV, Fig. 14) was somewhat overestimated; (c) the tail currents after depolarizations to large potentials were much slower than predicted by the model. These differences may represent uncertainties in our data at high $[\text{Ca}^{2+}]_i$ and large depolarizations (see Figs. 2 and 14) and/or may suggest a more complex gating mechanism, perhaps involving a third Ca^{2+} ion as suggested by the largest Hill coefficient of 2.4. Future experiments designed explicitly to address these issues may provide the data for a refinement in our understanding of the mechanism of Cl^- channel activation by Ca^{2+} ions. For now, the mechanism as embodied in Scheme I appears adequate to account for the major features of the Ca^{2+} -activated Cl^- channels in rat parotid acinar cells.

Physiological Role of the Ca^{2+} -activated Cl^- Channel

In a resting rat parotid acinar cell, the $[\text{Ca}^{2+}]_i$ is ~ 30 – 40 nM, and the membrane potential is near -60 mV. We have previously proposed that, under these conditions, the Ca^{2+} -dependent Cl^- channels are inactive (Arreola et al., 1996). However, during muscarinic cholinergic stimulation, the $[\text{Ca}^{2+}]_i$ can rise to levels as

high as 1,000 nM (Foskett and Melvin, 1989) with little change in the membrane potential (Nishiyama and Petersen, 1974; Nauntofte and Dissing, 1988). Such high $[\text{Ca}^{2+}]_i$ will induce a large activation of Cl^- current at negative voltages (see Fig. 3). The net result will be an enhancement of the apical Cl^- efflux as $[\text{Ca}^{2+}]_i$ increases.

It appears that the whole-cell currents measured at potentials close to those observed during muscarinic stimulation can account for the Cl^- loss. In the first 10 s, muscarinic stimulation induces a 50% Cl^- loss of the resting internal $[\text{Cl}^-]$ (~ 60 mM) (Foskett, 1990). This is equivalent to 45 fmol Cl^- /cell assuming a cell volume of 1.51 pl as predicted from capacitance measurements (comparable to volume estimated from cross-sectional areas). From Fig. 4 A, the average whole-cell current at -66 mV and 300 nM intracellular $[\text{Ca}^{2+}]_i$ was ~ -0.4 nA. The integration of this current over a 10-s period gave a charge of 4 nC, which is equivalent to 41 fmol Cl^- /cell. Thus, assuming that Ca^{2+} -dependent Cl^- channels in rat parotid acinar cells are mainly located in the apical membrane as has been shown in rat lacrimal cells (Tan et al., 1992), the Cl^- loss through Ca^{2+} -dependent Cl^- channels can explain almost 90% of the Cl^- loss observed during muscarinic receptor stimulation.

The evidence presented in this paper supports the view that Ca^{2+} -dependent Cl^- channels in rat parotid acinar cells are the predominant Cl^- efflux pathway activated during fluid and electrolyte secretion. Further studies to determine the mechanisms that control the activity of this channel and, finally, to establish its location in exocrine acinar cells are required to resolve unequivocally its role in the fluid secretion process.

We thank Drs. T. Shuttleworth and P. Stampe and Mrs. Jill Thompson for their critical reading of the manuscript.

This work was supported in part by National Institutes of Health grant DE09692.

Original version received 26 January 1996 and accepted version received 17 April 1996.

REFERENCES

- Anderson, M.P., D.N. Sheppard, H.A. Berger, and M.J. Welsh. 1992. Chloride channels in the apical membrane of normal and cystic fibrosis airway and intestinal epithelia. *Am. J. Physiol.* 263: L1-L14.
- Anderson, M.P., and M.J. Welsh. 1991. Calcium and cAMP activate different chloride channels in the apical membrane of normal and cystic fibrosis epithelia. *Proc. Natl. Acad. Sci. USA.* 88:6003-6007.
- Arreola, J., J.E. Melvin, and T. Begenisich. 1995a. Inhibition of Ca^{2+} -dependent Cl^- channels from secretory epithelial cells by low internal pH. *J. Membr. Biol.* 147:95-104.
- Arreola, J., J.E. Melvin, and T. Begenisich. 1995b. Volume-activated chloride channels in rat parotid acinar cells. *J. Physiol. (Camb.)* 484:677-687.
- Arreola, J., K. Park, J.E. Melvin, and T. Begenisich. 1996. Three chloride channels control Cl^- movements in rat parotid acinar cells. *J. Physiol. (Camb.)* 490:351-362.
- Cliff, W.H., and R.A. Frizzell. 1990. Separate Cl^- conductances activated by cAMP and Ca^{2+} in Cl^- -secreting epithelial cells. *Proc. Natl. Acad. Sci. USA.* 87:4956-4960.
- Cook, D.I., M.L. Day, M.P. Champion, and J.A. Young. 1988. Ca^{2+} not cAMP mediates the fluid secretory response to isoproterenol in the rat submandibular salivary gland: whole-cell patch-clamp studies. *Pflügers Arch. Eur. J. Physiol.* 413:67-76.
- Cook, D.I., E.W. Van Lennep, M.L. Roberts, and J.A. Young. 1994. Secretion by the major salivary glands. *In Physiology of the Gas-*

- trointestinal Tract. L.R. Johnson, editor. Raven Press, NY. 1061–1103.
- Douglas, W.W., and A.M. Poisner. 1963. The influence of calcium on the secretory response of the submaxillary gland to acetylcholine or to noradrenaline. *J. Physiol. (Camb.)*. 165:528–541.
- Evans, M.G., and A. Marty. 1986. Calcium-dependent chloride currents in isolated cells from rat lacrimal glands. *J. Physiol. (Camb.)*. 378:437–460.
- Foskett, J.K. 1990. $[Ca^{2+}]_i$ modulation of Cl^- content controls cell volume in single salivary acinar cells during fluid secretion. *Am. J. Physiol.* 259:C998–C1004.
- Foskett, J.K., and J.E. Melvin. 1989. Activation of salivary secretion: coupling of $[Ca^{2+}]_i$ and cell volume. *Science (Wash. DC)*. 244:1582–1585.
- Frizzell, R.A., and D.R. Halm. 1990. Chloride channels in epithelial cells. *Curr. Top. Membr. Transp.* 37:247–282.
- Goldman, D.E. 1943. Potential, impedance, and rectification in membranes. *J. Gen. Physiol.* 27:37–60.
- Gray, P.T.A. 1989. The relation of elevation of cytosolic free calcium to activation of membrane conductance in rat parotid acinar cells. *Proc. R. Soc. (Lond.) Ser. B Biol. Sci.* B237:99–107.
- Hamill, O.P., A. Marty, E. Neher, B. Sakmann, and F.J. Sigworth. 1981. Improved patch-clamp techniques for high-resolution current recording from cells and cell-free membrane patches. *Pflügers Arch. Eur. J. Physiol.* 391:85–100.
- Hodgkin, A.L., and B. Katz. 1949. The effect of sodium ions on the electrical activity of the giant axon of the squid. *J. Physiol. (Camb.)*. 108:37–77.
- Ishikawa, T., and D.I. Cook. 1993. A Ca^{2+} -activated Cl^- current in sheep parotid secretory cells. *J. Membr. Biol.* 135:261–271.
- Iwatsuki, N., Y. Maruyama, O. Matsumoto, and A. Nishiyama. 1985. Activation of Ca^{2+} -dependent Cl^- and K^+ conductances in rat and mouse parotid acinar cells. *Jpn. J. Physiol.* 35:933–944.
- Iwatsuki, N., and O.H. Petersen. 1977. Pancreatic acinar cells: the acetylcholine equilibrium potential and its ionic dependency. *J. Physiol. (Camb.)*. 269:735–751.
- Koumi, S., R. Sato, and T. Aramaki. 1994. Characterization of the calcium-activated chloride channel in isolated guinea-pig hepatocytes. *J. Gen. Physiol.* 104:357–373.
- Martinez, J.R., and N. Cassity. 1986. ^{36}Cl fluxes in dispersed rat submandibular acini: effects of Ca^{2+} omission and of the ionophore A23187. *Pflügers Arch. Eur. J. Physiol.* 407:615–619.
- Martinez, J.R., N. Cassity, and P. Red. 1987. An examination of functional linkage between K efflux and ^{36}Cl efflux in rat submandibular acini *in vitro*. *Arch. Oral Biol.* 32:891–895.
- Marty, A., and E. Neher. 1995. Tight-seal whole cell recording. In *Single-Channel Recording*. B. Sakmann and E. Neher, editors. Plenum Press, NY. 31–52.
- Melvin, J.E., M. Kawaguchi, B.J. Baum, and R.J. Turner. 1987. A muscarinic agonist-stimulated chloride efflux pathway is associated with fluid secretion in rat parotid acinar cells. *Biochem. Biophys. Res. Commun.* 145:754–759.
- Merritt, J.E., and T.J. Rink. 1987. Rapid increases in cytosolic free calcium in response to muscarinic stimulation in rat parotid acinar cells. *J. Biol. Chem.* 262:4958–4960.
- Nauntofte, B. 1992. Regulation of electrolyte and fluid secretion in salivary acinar cells. *Am. J. Physiol.* 263:C823–C837.
- Nauntofte, B., and S. Dissing. 1988. K^+ transport and membrane potentials in isolated rat parotid acini. *Am. J. Physiol.* 255:C508–C518.
- Nishiyama, A., and O.H. Petersen. 1974. Membrane potential and resistance measurement in acinar cells from salivary glands *in vitro*: effect of acetylcholine. *J. Physiol. (Camb.)*. 242:173–188.
- Overholt, J.L., M.E. Hobert, and R.D. Harvey. 1993. On the mechanism of rectification of the isoproterenol-activated chloride current in guinea-pig ventricular myocytes. *J. Gen. Physiol.* 102:871–895.
- Park, K., and P.D. Brown. 1995. Intracellular pH modulates the activity of chloride channels in isolated lacrimal gland acinar cells. *Am. J. Physiol.* 268:C647–C650.
- Petersen, O.H. 1992. Stimulus-secretion coupling: cytoplasmic calcium signals and the control of ion channels in exocrine acinar cells. *J. Physiol. (Camb.)*. 448:1–51.
- Petersen, O.H., and H.G. Philpott. 1980. Mouse pancreatic acinar cells: the anion selectivity of the acetylcholine-opened chloride pathway. *J. Physiol. (Camb.)*. 306:481–492.
- Pusch, M., U. Ludewig, A. Rehfeldt, and T.J. Jentsch. 1995. Gating of the voltage-dependent chloride channel $ClC-0$ by the permeant anion. *Nature (Lond.)*. 373:527–531.
- Sanchez, D.Y., and A.L. Blatz. 1992. Voltage-dependent block of fast chloride channels from rat cortical neurons by external tetraethylammonium ion. *J. Gen. Physiol.* 100:217–231.
- Tan, Y.P., A. Marty, and A. Trautmann. 1992. High density of Ca^{2+} -dependent K^+ and Cl^- channels on the luminal membrane of lacrimal acinar cells. *Proc. Natl. Acad. Sci. USA*. 89:11229–11233.
- Tsien, R., and T. Pozzan. 1989. Measurements of cytosolic free Ca^{2+} with Quin 2. *Methods Enzymol.* 172:230–262.
- Turner, R.J. 1993. Ion transport related to fluid secretion in salivary glands. In *Biology of the Salivary Glands*. K. Dobrosielski-Vergona, editor. CRC Press Inc. Salem, MA. 105–127.
- Woodhull, A.M. 1973. Ionic blockage of sodium channels in nerve. *J. Gen. Physiol.* 61:687–708.
- Worrell, R.T., and R.A. Frizzell. 1991. CaMKII mediates stimulation of chloride conductance by calcium in T84 cells. *Am. J. Physiol.* 260:C877–C882.
- Zhang, G., J. Arreola, and J.E. Melvin. 1995. Inhibition by thiocyanate of muscarinic-induced cytosolic acidification and Ca^{2+} entry in rat sublingual acini. *Arch. Oral Biol.* 40:111–118.